AIAA JOURNAL
Vol. 43, No. 6, June 2005

Power Flow Analysis of Complex Structures Using Characteristic Constraint Modes

Yung-Chang Tan,* Matthew P. Castanier,† and Christophe Pierre‡
University of Michigan, Ann Arbor, Michigan 48109-2125

Component mode synthesis (CMS) is used as a basis for predicting power flow in complex structures. The power flow formulation is cast in a general framework of multilevel CMS, in which a hierarchy of substructures can be recursively partitioned from a very large finite element model. Additional computational efficiency is achieved by finding characteristic constraint (CC) modes. The CC modes are computed by performing an eigenanalysis on the partitions of the CMS mass and stiffness matrices that correspond to the constraint-mode degrees of freedom. The CC modes describe the vibration, and the exchange of vibration energy, at the interface between connected substructures. Therefore, a relatively small number of CC modes that capture the primary interface motion can be selected to yield a reduced-order model for computing the power flow. The performance and accuracy of the method are illustrated by examples of a two-span beam, a cantilever plate, and the body structure of a military vehicle. For the vehicle structure, multiple levels of substructures are used to map the power flow in the system. It is seen that this multilevel, characteristic-mode-based approach provides a general framework for the efficient calculation of power flow in the low- to midfrequency range.

Nomenclature

$\boldsymbol{A}, \boldsymbol{\alpha}, \boldsymbol{\beta}$	=	Boolean matrix
$\boldsymbol{f}$	=	force vector
I	=	index set for a group of substructures
j	=	$\sqrt{-1}$
$\boldsymbol{K}$	=	stiffness matrix
$\boldsymbol{k}$	=	stiffness matrix partition
$\boldsymbol{M}$	=	mass matrix
$\boldsymbol{m}$	=	mass matrix partition
$\boldsymbol{S}$	=	power spectral density matrix
$\boldsymbol{T}, \boldsymbol{t}$	=	traction force vector
$\boldsymbol{v}$	=	velocity vector
$\boldsymbol{Y}$	=	mobility matrix
$\boldsymbol{Z}, \boldsymbol{z}$	=	impedance matrix
Γ	=	substructure interface domain
γ	=	structural damping factor
Θ	=	substructure interior-interface domain
λ_n	=	eigenvalue
Π_{ab}	=	power flow from substructure a to substructure b
$\boldsymbol{\Phi}^C$	=	full set of constraint modes
$\boldsymbol{\Phi}^N$	=	selected set of substructure normal modes
$\boldsymbol{\Psi}$	=	selected set of characteristic constraint modes
ψ_n	=	characteristic constraint mode
Ω	=	substructure interior domain
ω	=	frequency

Subscripts

a, b	=	index values for two connected substructures
h	=	index for a higher-level substructure
i	=	index for a bottom-level substructure

Superscripts

C	=	constraint-mode degree of freedom (DOF)
CC	=	characteristic-constraint-mode DOF
CMS	=	component mode synthesis model
N	=	normal-mode DOF
ROM	=	reduced-order model
Γ	=	interface DOF
Θ	=	interior-interface DOF
Ω	=	interior DOF

Received 28 March 2002; accepted for publication 27 October 2003.

*Graduate Student Research Assistant, Department of Mechanical Engineering; currently CAE Analyst, Analytical Powertrain Department, Ford Motor Company, Dearborn, MI 48121-4091.

†Associate Research Scientist, Department of Mechanical Engineering; mpc@umich.edu. Senior Member AIAA.

‡Stephen P. Timoshenko Collegiate Professor, Department of Mechanical Engineering; pierre@umich.edu. Senior Member AIAA.

Introduction

IN the vibration analysis of a complex structure, the analyst often needs to know how vibration in one part of the structure will be transmitted to other parts of the structure. This information can be provided by performing a power flow analysis: the complex structure is partitioned into component structures, and the amount of energy exchanged at each interface between connected components is determined.

There are various methods for predicting power flow in complex structures. In fact, the calculation of power flow is a core concept for statistical energy analysis[1,2] (SEA), in which a complex structure is modeled as a collection of interconnected subsystems. The application of SEA involves estimating the subsystem energies, modal densities, and the coupling between the subsystems. Although this approach is effective in the high-frequency range, it is known that the response statistics calculated from SEA might not give satisfactory predictions in the low- to midfrequency range.

For the low-frequency range, finite element analysis is accurate and reliable. However, it becomes computationally expensive in the midfrequency range because of the tremendous number of degrees of freedom (DOF) needed to capture the shorter wavelengths of vibration. To reduce the computational costs, component mode synthesis[3–5] (CMS) can be used. In CMS, a modal analysis is performed on each component finite element model (FEM), and then a reduced-order model (ROM) of the global structure is assembled. It was found by the authors[6] that the Craig–Bampton method[4] of CMS provides a good foundation for predicting power flow because the Craig–Bampton constraint modes capture fully the motion of the interface between component structures. However, because there is necessarily one constraint mode for each FEM DOF in the interface, the cost of this CMS method is still prohibitive for a sufficiently fine mesh.

In this paper, the size of the CMS model is reduced by employing a secondary modal analysis. For the purpose of predicting power flow, this secondary modal analysis is applied to the interface between components. In particular, an eigenanalysis is performed on the constraint-mode partitions of the CMS mass and stiffness matrices. The resultant eigenvectors, which describe the characteristic motion of the interface, are called characteristic constraint (CC) modes.[7] A subset of the CC modes can be selected for the frequency range of interest, thus reducing the size of the system model. Then, the power flow equations are derived such that the transmitted power is projected onto this lower-dimensional basis of CC modes. This formulation provides improved efficiency for the prediction of vibration transmission in the low- to midfrequency range. Furthermore, this technique is extended to multilevel substructuring, in which the initial component structures are divided recursively into lower-level substructures. This can be used to handle very large FEMs, and the power flow can be computed at each level of substructures. As a result, a power flow map can be constructed to identify the critical vibration transmission paths and the parts with severe vibration.

There has been previous work on developing interface reduction techniques for CMS. Craig and Chang[8] summarized fixed-interface and free-interface methods of substructure coupling for dynamic analysis, and they introduced techniques for reducing interface DOF for fixed-interface CMS methods. Bourquin and d'Hennezel[9,10] proposed numerical methods to seek alternative constraint modes called the "coupling modes." Balmès[11] tried to select optimal Ritz vectors by applying singular value decomposition based on the strain and kinetic energy norm. Brahmi and Bouhaddi[12] applied a generalized Guyan reduction method on the CMS matrices to reduce the interface DOF. In addition, the technique of multilevel substructuring, or the recursive application of CMS to multiple levels of substructures, has been used to reduce both substructure and system analysis costs.[13–20] Most notably, Bennighof and coworkers[16–19] have developed an automated multilevel substructuring method, which allows large FEMs to be divided automatically into thousands of substructures on dozens of levels. However, none of these modeling techniques was used as a basis for power flow analysis. In contrast, the CC-mode-based method presented in this paper is designed to determine the power flow between the component structures, as well as to provide physical insight into how the vibration energy propagates.

Finally, it is noted that other finite element-based methods have been developed for analyzing power flow. For example, in an approach called power flow finite element analysis or energy finite element analysis, the flow of mechanical energy is modeled in a manner that is analogous to the flow of thermal energy in heat conduction.[21–23] Some energy flow models have been developed for structural elements such as beams and plates with certain propagating wave modes. However, it is believed that the power flow technique presented in this paper is more widely applicable, straightforward, and accurate in the low- to midfrequency range. More recently, Mace and Shorter[24] applied fixed-interface CMS techniques to FEMs in order to investigate power flow. However, instead of using the direct formulation for calculating power flow over the interface substructure energy and power input were computed, and thus the energy influence coefficients between the substructures were determined. In contrast, the approach outlined in the present study provides additional computational efficiency and physical insight by using CC modes to describe the interface motion.

This paper is organized as follows. In the second section, the CMS and CC mode techniques are summarized in the context of multilevel substructuring, and a CC-mode-based reduced-order model is constructed for computing the power flow. In the third section, modal approximations of power flow using the reduced-order model are presented in detail. In the fourth section, a two-span beam and a cantilever plate are used as example systems to illustrate the accuracy and efficiency of the power flow formulation. In the fifth section, the technique of multilevel substructuring is applied to the body structure a military vehicle, and power flow is calculated at each level. In the final section, this work is summarized and concluded.

Multilevel CMS with Characteristic Constraint Modes

In CMS, the finite element model of a structure is divided into a number of substructures. The choice of component structures might be obvious in some cases, but there are several considerations that can dictate the partitioning plan. For example, because power flow is calculated at the interface between connected components, the flow of vibration energy can be tracked through critical regions of the structure by defining the substructures accordingly. Furthermore, after an initial partitioning the substructure FEMs might still have a large number of DOF and be computationally cumbersome. For very large FEMs, it might be helpful to divide each component structure into another set of substructures, to reduce the cost of the finite element analysis needed to compute component modes and constraint modes. This multilevel substructuring approach[13–20] results in a hierarchy of component structure levels. In this study, the original system is considered to be at the top, and each partitioning results in a lower level of substructures:

1) The entire system is considered to be the top-level substructure.

2) The top-level substructure is divided into a set of intermediate-level substructures, which then can be partitioned recursively into lower levels of intermediate-level substructures.

3) Substructures that are not partitioned further are called bottom-level substructures.

After this multilevel partitioning, the Craig–Bampton method[4] of CMS is used to synthesize the bottom-level substructures into models of the intermediate-level substructures that are one level higher. These intermediate-level models are then synthesized into models of the next-higher-level substructures, and so forth. Eventually, a model is assembled for the top-level substructure, which is the full system. The CC modes[7] can be used to reduce the model size and support the calculation of power flow at any or all levels of substructuring. This process is covered in the following subsections.

Equations of Motion for Bottom-Level Substructures

After the finite element discretization, the equations of steady-state motion for bottom-level substructure i can be written as

$$(1/j\omega)\left[-\omega^2 \boldsymbol{M}_i + (1 + j\gamma)\boldsymbol{K}_i\right]\boldsymbol{v}_i(\omega) = \boldsymbol{T}_i(\omega) + \boldsymbol{f}_i(\omega) \quad \text{for} \quad i \in I \tag{1}$$

where $\boldsymbol{I}$ is the index set of the adjacent substructures that constitute the higher-level substructure h, $\boldsymbol{M}_i$ is the substructure mass matrix, $\boldsymbol{K}_i$ is the substructure stiffness matrix, $\boldsymbol{T}_i$ is the traction force, and $\boldsymbol{f}_i$ is the applied force. The unknowns $\boldsymbol{v}_i$ are the physical velocities of the nodal grid points. The velocities are used instead of displacements because the velocities are needed to formulate the power flow.

Let Ω_i be a three-dimensional, open, bounded, connected domain occupied by the component structure labeled by index i. Let $\partial\Omega_i$ be the boundary of Ω_i (assumed to be smooth), Γ_i the interface with adjacent substructures, and Σ_i the fixed boundary with displacement $\boldsymbol{u}_i^{\Sigma} = 0$, such that $\partial\Omega_i = \Gamma_i \cup \Sigma_i$ with $\Gamma_i \cap \Sigma_i = \emptyset$. The velocities $\boldsymbol{v}_i$ are now partitioned into interface and interior DOF:

$$\boldsymbol{v}_i = \begin{Bmatrix} \boldsymbol{v}_i^{\Gamma} \\ \boldsymbol{v}_i^{\Omega} \end{Bmatrix} \tag{2}$$

where $\boldsymbol{v}_i^{\Gamma}$ are the velocities of the interface Γ_i and $\boldsymbol{v}_i^{\Omega}$ are the velocities on domain Ω_i. Correspondingly, $\boldsymbol{M}_i$, $\boldsymbol{K}_i$, $\boldsymbol{T}_i$, and $\boldsymbol{f}_i$ can be partitioned as follows:

$$\boldsymbol{M}_i = \begin{bmatrix} \boldsymbol{m}_i^{\Gamma\Gamma} & \boldsymbol{m}_i^{\Gamma\Omega} \\ \boldsymbol{m}_i^{\Omega\Gamma} & \boldsymbol{m}_i^{\Omega\Omega} \end{bmatrix}, \qquad \boldsymbol{K}_i = \begin{bmatrix} \boldsymbol{k}_i^{\Gamma\Gamma} & \boldsymbol{k}_i^{\Gamma\Omega} \\ \boldsymbol{k}_i^{\Omega\Gamma} & \boldsymbol{k}_i^{\Omega\Omega} \end{bmatrix} \tag{3}$$

$$\boldsymbol{T}_i = \begin{Bmatrix} \boldsymbol{t}_i \\ 0 \end{Bmatrix}, \qquad \boldsymbol{f}_i = \begin{Bmatrix} \boldsymbol{f}_i^{\Gamma} \\ \boldsymbol{f}_i^{\Omega} \end{Bmatrix} \tag{4}$$

where the unknown interface tractions $\boldsymbol{t}_i$ will be eliminated after coupling the subsystem equations to form the system equations.

The Craig–Bampton method[4] of component mode synthesis utilizes two sets of substructure modes: component normal modes $\boldsymbol{\Phi}_i^N$ and constraint modes $\boldsymbol{\Phi}_i^C$. The component normal modes are the normal modes of a substructure with all DOF of the interface held fixed. A constraint mode is the static deflection induced in a substructure by applying a unit displacement to one interface DOF while all other interface DOF are held fixed. The constraint modes provide a complete and mathematically convenient set of deformation shapes associated with the motion of the interface DOF. The interior finite element DOF $\boldsymbol{v}_i^\Omega$, thus can be represented by the constraint mode DOF $\boldsymbol{v}_i^C$ and the normal mode DOF $\boldsymbol{v}_i^N$ by the following form:

$$\boldsymbol{v}_i^\Omega = \boldsymbol{\Phi}_i^C \boldsymbol{v}_i^C + \boldsymbol{\Phi}_i^N \boldsymbol{v}_i^N \tag{5}$$

Hence

$$\begin{Bmatrix} \boldsymbol{v}_i^\Gamma \\ \boldsymbol{v}_i^\Omega \end{Bmatrix} = \begin{bmatrix} \boldsymbol{I} & 0 \\ \boldsymbol{\Phi}_i^C & \boldsymbol{\Phi}_i^N \end{bmatrix} \begin{Bmatrix} \boldsymbol{v}_i^C \\ \boldsymbol{v}_i^N \end{Bmatrix} \tag{6}$$

Note that $\boldsymbol{v}_i^\Gamma = \boldsymbol{v}_i^C$. Equation (1) can be transformed to

$$(1/j\omega)\left[-\omega^2 \tilde{\boldsymbol{M}}_i + (1 + j\gamma)\tilde{\boldsymbol{K}}_i\right]\tilde{\boldsymbol{v}}_i = \boldsymbol{T}_i + \tilde{\boldsymbol{f}}_i, \qquad i \in I \tag{7}$$

where

$$\tilde{\boldsymbol{v}}_i = \begin{Bmatrix} \boldsymbol{v}_i^C \\ \boldsymbol{v}_i^N \end{Bmatrix} \tag{8}$$

The mass and stiffness matrices and the applied modal force vector are now of the form

$$\tilde{\boldsymbol{M}}_i = \begin{bmatrix} \boldsymbol{m}_i^C & \boldsymbol{m}_i^{CN} \\ \boldsymbol{m}_i^{CN^T} & \boldsymbol{m}_i^N \end{bmatrix} \tag{9}$$

$$\tilde{\boldsymbol{K}}_i = \begin{bmatrix} \boldsymbol{k}_i^C & 0 \\ 0 & \boldsymbol{k}_i^N \end{bmatrix} \tag{10}$$

$$\tilde{\boldsymbol{f}}_i = \begin{Bmatrix} \boldsymbol{f}_i^C \\ \boldsymbol{f}_i^N \end{Bmatrix} \tag{11}$$

Note that the normal mode submatrices $\boldsymbol{m}_i^N$ and $\boldsymbol{k}_i^N$ are diagonal.

CMS for Higher-Level Substructures

The substructures in the index set I are now connected to form higher-level substructure h (which can be the top-level substructure or just an intermediate-level substructure) via the interface DOF on $\bigcup_{i \in I} \Gamma_i$. The following transformation is considered:

$$\boldsymbol{v}_i^C = \boldsymbol{\beta}_i^C \boldsymbol{v}_h^C \tag{12}$$

where $\boldsymbol{\beta}_i^C$ is the Boolean matrix that maps the global interface coordinates $\boldsymbol{v}_h^C$ back to the local coordinates $\boldsymbol{v}_i^C$. The interface partitions of the CMS stiffness and mass matrices of substructure h are given by

$$\bar{\boldsymbol{m}}_h^C = \sum_{i \in I} \boldsymbol{\beta}_i^{C^T} \boldsymbol{m}_i^C \boldsymbol{\beta}_i^C \tag{13}$$

$$\bar{\boldsymbol{k}}_h^C = \sum_{i \in I} \boldsymbol{\beta}_i^{C^T} \boldsymbol{k}_i^C \boldsymbol{\beta}_i^C \tag{14}$$

Assuming that there are s substructures in the index set I, the global velocities of substructure h are formulated as

$$\boldsymbol{v}_h^{CMS} = \begin{bmatrix} \boldsymbol{v}_h^{C^*} & \boldsymbol{v}_{i_1}^{N^*} & \boldsymbol{v}_{i_2}^{N^*} & \cdots & \boldsymbol{v}_{i_s}^{N^*} \end{bmatrix}^* \tag{15}$$

where $*$ denotes a complex conjugate transpose. The equations of motion of the synthesized CMS model for substructure h are expressed by

$$(1/j\omega)\left[-\omega^2 \boldsymbol{M}_h^{CMS} + (1 + j\gamma)\boldsymbol{K}_h^{CMS}\right]\boldsymbol{v}_h^{CMS} = \boldsymbol{T}_h^{CMS} + \boldsymbol{f}_h^{CMS} \tag{16}$$

The corresponding CMS mass and stiffness matrices of substructure h are represented by

$$\boldsymbol{M}_h^{CMS} = \begin{bmatrix} \bar{\boldsymbol{m}}_h^C & \boldsymbol{m}_{i_1}^{CN} & \boldsymbol{m}_{i_2}^{CN} & \cdots & \boldsymbol{m}_{i_s}^{CN} \\ \boldsymbol{m}_{i_1}^{CN^T} & \boldsymbol{m}_{i_1}^N & 0 & \cdots & 0 \\ \boldsymbol{m}_{i_2}^{CN^T} & 0 & \boldsymbol{m}_{i_2}^N & & 0 \\ \vdots & \vdots & & \ddots & \vdots \\ \boldsymbol{m}_{i_s}^{CN^T} & 0 & 0 & \cdots & \boldsymbol{m}_{i_s}^N \end{bmatrix} \tag{17}$$

$$\boldsymbol{K}_h^{CMS} = \begin{bmatrix} \bar{\boldsymbol{k}}_h^C & 0 & 0 & \cdots & 0 \\ 0 & \boldsymbol{k}_{i_1}^N & 0 & \cdots & 0 \\ 0 & 0 & \boldsymbol{k}_{i_2}^N & & 0 \\ \vdots & \vdots & & \ddots & \vdots \\ 0 & 0 & 0 & \cdots & \boldsymbol{k}_{i_s}^N \end{bmatrix} \tag{18}$$

The force vector is

$$\boldsymbol{f}_h^{CMS} = \begin{bmatrix} \bar{\boldsymbol{f}}_h^{C^*} & \boldsymbol{f}_{i_1}^{N^*} & \boldsymbol{f}_{i_2}^{N^*} & \cdots & \boldsymbol{f}_{i_s}^{N^*} \end{bmatrix}^* \tag{19}$$

where

$$\bar{\boldsymbol{f}}_h^C = \sum_{i \in I} \boldsymbol{\beta}_i^{C^T} \boldsymbol{f}_i^C \tag{20}$$

For an intermediate-level substructure h, the interface domain $\bigcup_{i \in I} \Gamma_i$ is partitioned into Γ_h and Θ_h, where Γ_h is the new interface with adjacent substructures, while Θ_h becomes part of the interior domain such that $\Omega_h = (\bigcup_{i \in I} \Omega_i) \cup \Theta_h$. The domain Θ_h is referred to as the interior interface because it contains the interface between the connected lower-level substructures that comprise substructure h. Furthermore, Θ_h is the region where the power flow is computed. This partitioning can also be applied to the top-level substructure, which does not have an interface with other substructures, yielding $\Theta_h = \bigcup_{i \in I} \Gamma_i$ and $\Gamma_h = \emptyset$.

Using these domain definitions, the Boolean matrix $\boldsymbol{\beta}_i^C$ and the velocities $\boldsymbol{v}_h^C$ can be partitioned such that Eq. (12) becomes

$$\boldsymbol{v}_i^C = \begin{bmatrix} \boldsymbol{\beta}_i^\Gamma & 0 \\ 0 & \boldsymbol{\beta}_i^\Theta \end{bmatrix} \begin{bmatrix} \boldsymbol{v}_h^\Gamma \\ \boldsymbol{v}_h^\Theta \end{bmatrix} \tag{21}$$

Note that the following coupling condition is imposed when assembling the component equations into Eq. (16):

$$\sum_{i \in I} \boldsymbol{\beta}_i^{\Theta^T} \boldsymbol{t}_i = 0 \tag{22}$$

Then, $\bar{\boldsymbol{m}}_h^C$, $\boldsymbol{m}_i^{CN}$, and $\bar{\boldsymbol{k}}_h^C$ in Eqs. (17) and (18) are partitioned as

$$\bar{\boldsymbol{m}}_h^C = \begin{bmatrix} \boldsymbol{m}_h^{\Gamma\Gamma} & \boldsymbol{m}_h^{\Gamma\Theta} \\ \boldsymbol{m}_h^{\Gamma\Theta^T} & \boldsymbol{m}_h^{\Theta\Theta} \end{bmatrix} \tag{23}$$

$$\boldsymbol{m}_i^{CN} = \begin{bmatrix} \boldsymbol{m}_i^{\Gamma N} \\ \boldsymbol{m}_i^{\Theta N} \end{bmatrix} \tag{24}$$

$$\bar{\boldsymbol{k}}_h^C = \begin{bmatrix} \boldsymbol{k}_h^{\Gamma\Gamma} & \boldsymbol{k}_h^{\Gamma\Theta} \\ \boldsymbol{k}_h^{\Gamma\Theta^T} & \boldsymbol{k}_h^{\Theta\Theta} \end{bmatrix} \tag{25}$$

To apply the CMS transformation, interface and interior partitions and their coupling terms are needed. That is, Eqs. (17) and (18) need to be repartitioned as

$$\boldsymbol{M}_h^{CMS} = \begin{bmatrix} \boldsymbol{m}_h^{\Gamma\Gamma} & \boldsymbol{m}_h^{\Gamma\Omega} \\ \boldsymbol{m}_h^{\Omega\Gamma} & \boldsymbol{m}_h^{\Omega\Omega} \end{bmatrix}, \qquad \boldsymbol{K}_h^{CMS} = \begin{bmatrix} \boldsymbol{k}_h^{\Gamma\Gamma} & \boldsymbol{k}_h^{\Gamma\Omega} \\ \boldsymbol{k}_h^{\Omega\Gamma} & \boldsymbol{k}_h^{\Omega\Omega} \end{bmatrix}$$

The interface partitions $\boldsymbol{m}_h^{\Gamma\Gamma}$ and $\boldsymbol{k}_h^{\Gamma\Gamma}$ are obtained from Eqs. (23) and (25). The interior partitions are defined by

$$\boldsymbol{m}_h^{\Omega\Omega} = \begin{bmatrix} \boldsymbol{m}_h^{\Theta\Theta} & \boldsymbol{m}_{i_1}^{\Theta N} & \cdots & \boldsymbol{m}_{i_s}^{\Theta N} \\ \boldsymbol{m}_{i_1}^{\Theta N^T} & \boldsymbol{m}_{i_1}^{N} & 0 & 0 \\ \vdots & 0 & \ddots & 0 \\ \boldsymbol{m}_{i_s}^{\Theta N^T} & 0 & 0 & \boldsymbol{m}_{i_s}^{N} \end{bmatrix} \tag{26}$$

$$\boldsymbol{k}_h^{\Omega\Omega} = \begin{bmatrix} \boldsymbol{k}_h^{\Theta\Theta} & 0 & 0 & 0 \\ 0 & \boldsymbol{k}_{i_1}^{N} & 0 & 0 \\ 0 & 0 & \ddots & 0 \\ 0 & 0 & 0 & \boldsymbol{k}_{i_s}^{N} \end{bmatrix} \tag{27}$$

The coupling submatrices are defined by

$$\boldsymbol{m}_h^{\Gamma\Omega} = \boldsymbol{m}_h^{\Omega\Gamma^T} = \begin{bmatrix} \boldsymbol{m}_h^{\Gamma\Theta} & \boldsymbol{m}_{i_1}^{\Gamma N} & \cdots & \boldsymbol{m}_{i_s}^{\Gamma N} \end{bmatrix} \tag{28}$$

$$\boldsymbol{k}_h^{\Gamma\Omega} = \boldsymbol{k}_h^{\Omega\Gamma^T} = \begin{bmatrix} \boldsymbol{k}_h^{\Gamma\Theta} & 0 & \cdots & 0 \end{bmatrix} \tag{29}$$

Correspondingly, the velocity vector for Ω_h is represented by

$$\boldsymbol{v}_h^{\Omega} = \begin{bmatrix} \boldsymbol{v}_h^{\Theta^*} & \boldsymbol{v}_{i_1}^{N^*} & \boldsymbol{v}_{i_2}^{N^*} & \cdots & \boldsymbol{v}_{i_s}^{N^*} \end{bmatrix}^* \tag{30}$$

and the force vector for Ω_h is represented by

$$\boldsymbol{f}_h^{\Omega} = \begin{bmatrix} \boldsymbol{f}_h^{\Theta^*} & \boldsymbol{f}_{i_1}^{N^*} & \boldsymbol{f}_{i_2}^{N^*} & \cdots & \boldsymbol{f}_{i_s}^{N^*} \end{bmatrix}^* \tag{31}$$

where $\boldsymbol{f}_h^{\Theta}$ is taken from

$$\bar{\boldsymbol{f}}_h^{C} = \begin{bmatrix} \boldsymbol{f}_h^{\Gamma^*} & \boldsymbol{f}_h^{\Theta^*} \end{bmatrix}^* \tag{32}$$

Next, for an intermediate-level substructure the component normal modes $\boldsymbol{\Phi}_h^N$ and the constraint modes $\boldsymbol{\Phi}_h^C$ are calculated. Following the CMS transformation, Eq. (6), a reduced-order model for substructure h with exactly the same form as Eq. (7) can be obtained. The transformation for this substructure model h is now complete and ready to be connected to other bottom- or intermediate-level substructure models through its interface coordinates $\boldsymbol{v}_h^{\Gamma}$. The process described in this subsection can then be repeated by allowing the substructure index set I to include the indices of bottom- and intermediate-level substructures.

Characteristic Constraint Modes

If substructure h is the top-level substructure, Eq. (16) is reduced to

$$(1/j\omega)\left[-\omega^2 \boldsymbol{m}_h^{\Omega\Omega} + (1 + j\gamma)\boldsymbol{k}_h^{\Omega\Omega}\right]\boldsymbol{v}_h^{\Omega} = \boldsymbol{f}_h^{\Omega} \tag{33}$$

However, if substructure h is an intermediate-level substructure, the equations of motion become

$$(1/j\omega)\left[-\omega^2 \boldsymbol{m}_h^{\Omega\Omega} + (1 + j\gamma)\boldsymbol{k}_h^{\Omega\Omega}\right]\boldsymbol{v}_h^{\Omega} = \boldsymbol{f}_h^{\Omega} - (1/j\omega)\left[-\omega^2 \boldsymbol{m}_h^{\Omega\Gamma} + (1 + j\gamma)\boldsymbol{k}_h^{\Omega\Gamma}\right]\boldsymbol{v}_h^{\Gamma} \tag{34}$$

Because $\boldsymbol{v}_h^{\Gamma}$ will be solved from the equations of motion of the higher-level substructure for each frequency ω, the right-hand side of Eq. (34) can be treated as a modified force vector $\bar{\boldsymbol{f}}_h^{\Omega}$:

$$\bar{\boldsymbol{f}}_h^{\Omega} = \boldsymbol{f}_h^{\Omega} - (1/j\omega)\left[-\omega^2 \boldsymbol{m}_h^{\Omega\Gamma} + (1 + j\gamma)\boldsymbol{k}_h^{\Omega\Gamma}\right]\boldsymbol{v}_h^{\Gamma} \tag{35}$$

The velocities $\boldsymbol{v}_h^{\Omega}$ need to be solved from Eqs. (33) or (34) at each frequency in order to retrieve $\boldsymbol{v}_h^{\Theta}$ [see Eq. (30)] and then calculate the power flow. The size of $\boldsymbol{v}_h^{\Theta}$ is equal to the number of FEM DOF in the interior interface n^{Θ}, which is determined by the finite element mesh. If the mesh is fine in the interface regions or if there are several substructures, the corresponding partitions of the CMS matrices might be relatively large. Hence, the authors proposed a technique[7] to further reduce the CMS model by performing a modal analysis on the Θ_h partitions of the CMS matrices

$$\boldsymbol{k}_h^{\Theta\Theta}\psi_n = \lambda_n \boldsymbol{m}_h^{\Theta\Theta}\psi_n \qquad \text{for} \qquad n = 1, 2, \ldots, n^{\Theta} \tag{36}$$

which yields the characteristic constraint modes. A subset of CC modes $\boldsymbol{\Psi}_h$ can be selected as in a traditional modal analysis. One key application of CC modes is for the efficient computation of power flow at the interface between connected component structures. Relatively few CC-mode DOF are employed in this calculation compared to the number of interface DOF in the FEM.

The transformation from CC-mode coordinates to constraint-mode coordinates is defined as

$$\boldsymbol{v}_h^{\Theta} = \boldsymbol{\Psi}_h \boldsymbol{v}_h^{CC} \tag{37}$$

The equations of motion of the ROM are expressed by

$$\frac{1}{j\omega}\left[-\omega^2 \boldsymbol{M}_h^{\mathrm{ROM}} + (1 + j\gamma)\boldsymbol{K}_h^{\mathrm{ROM}}\right]\boldsymbol{v}_h = \boldsymbol{f}_h^{\mathrm{ROM}} \tag{38}$$

The ROM mass and stiffness matrices are of the form

$$\boldsymbol{M}_h^{\mathrm{ROM}} = \begin{bmatrix} \bar{\boldsymbol{m}}_h^{CC} & \bar{\boldsymbol{m}}_{i_1}^{CN} & \bar{\boldsymbol{m}}_{i_2}^{CN} & \cdots & \bar{\boldsymbol{m}}_{i_s}^{CN} \\ \bar{\boldsymbol{m}}_{i_1}^{CN^T} & \boldsymbol{m}_{i_1}^{N} & 0 & \cdots & 0 \\ \bar{\boldsymbol{m}}_{i_2}^{CN^T} & 0 & \boldsymbol{m}_{i_2}^{N} & & 0 \\ \vdots & \vdots & & \ddots & \vdots \\ \bar{\boldsymbol{m}}_{i_s}^{CN^T} & 0 & 0 & \cdots & \boldsymbol{m}_{i_s}^{N} \end{bmatrix} \tag{39}$$

$$\boldsymbol{K}_h^{\mathrm{ROM}} = \begin{bmatrix} \bar{\boldsymbol{k}}_h^{CC} & 0 & 0 & \cdots & 0 \\ 0 & \boldsymbol{k}_{i_1}^{N} & 0 & \cdots & 0 \\ 0 & 0 & \boldsymbol{k}_{i_2}^{N} & & 0 \\ \vdots & \vdots & & \ddots & \vdots \\ 0 & 0 & 0 & \cdots & \boldsymbol{k}_{i_s}^{N} \end{bmatrix} \tag{40}$$

where

$$\bar{\boldsymbol{m}}_h^{CC} = \boldsymbol{\Psi}_h^T \bar{\boldsymbol{m}}_h^{\Theta\Theta} \boldsymbol{\Psi}_h, \qquad \bar{\boldsymbol{k}}_h^{CC} = \boldsymbol{\Psi}_h^T \bar{\boldsymbol{k}}_h^{\Theta\Theta} \boldsymbol{\Psi}_h \tag{41}$$

Note that $\bar{\boldsymbol{m}}_h^{CC}$ and $\bar{\boldsymbol{k}}_h^{CC}$ are diagonal matrices, as follows from Eq. (36). The coupling submatrices $\bar{\boldsymbol{m}}_i^{CN}$ are given by

$$\bar{\boldsymbol{m}}_i^{CN} = \boldsymbol{\Psi}_h^T \boldsymbol{\beta}_i^{\Theta^T} \boldsymbol{m}_i^{\Theta N} \tag{42}$$

The forcing vector $\boldsymbol{f}_h^{\mathrm{ROM}}$ is transformed from $\bar{\boldsymbol{f}}_h^{\Omega}$ or $\boldsymbol{f}_h^{\Omega}$ using the CC modes $\boldsymbol{\Psi}$, and it can be partitioned as

$$\boldsymbol{f}_h^{\mathrm{ROM}} = \begin{bmatrix} \bar{\boldsymbol{f}}_h^{CC^*} & \boldsymbol{f}_{i_1}^{N^*} & \boldsymbol{f}_{i_2}^{N^*} & \cdots & \boldsymbol{f}_{i_s}^{N^*} \end{bmatrix}^* \tag{43}$$

Approximations of Power Flow

The solution of the power flow requires first solving the system equations of the ROM, Eq. (38). It can be seen that the system mass matrix, Eq. (39), is doubly bordered band diagonal, whereas the system stiffness matrix, Eq. (40), is purely diagonal. The following derivation takes advantage of the sparsity of these matrices. To this end, the submatrices will be used explicitly for formulating the power flow.

Assume that substructures a and b are connected such that $a, b \in I$, which is the substructure index set of higher-level substructure h. The power flowing from substructure a to substructure b can be defined by

$$\Pi_{ab}(\omega) = -\frac{1}{2\pi} \lim_{T \to 0} \frac{1}{2T} E_t\left\{\mathrm{Re}\left[\boldsymbol{v}_a^C(\omega; T)^* \boldsymbol{\alpha}_{ab}^T \boldsymbol{\alpha}_{ab} \boldsymbol{t}_a(\omega; T)\right]\right\} \tag{44}$$

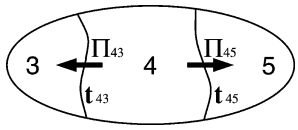

Fig. 1 Power flow and traction forces for three substructures.

where $E_t[\,]$ denotes the expected value with respect to time, $\boldsymbol{t}_a$ is the traction force vector, and $\boldsymbol{v}_a^C$ is the corresponding velocity vector on the interface. In most cases, a substructure is connected to more than one other substructure. Thus, $\boldsymbol{\alpha}_{ab}$ is employed in Eq. (44) to map the total interface DOF to the interface DOF between substructures a and b. For example, consider the substructures shown in Fig. 1. Substructure 4 is connected to substructures 3 and 5. Now let $a = 4$, $b = 3$, and assume that the traction force $\boldsymbol{t}_4$ can be partitioned as

$$\boldsymbol{t}_4 = \begin{Bmatrix} \boldsymbol{t}_{43} \\ \boldsymbol{t}_{45} \end{Bmatrix} \tag{45}$$

To find power flow Π_{43}, it is necessary to define $\boldsymbol{\alpha}_{43}$ as

$$\boldsymbol{\alpha}_{43} = \begin{bmatrix} \boldsymbol{I}_{n_{43}\times n_{43}} & 0_{n_{43}\times n_{45}} \end{bmatrix} \tag{46}$$

where n_{43} and n_{45} are the numbers of elements in vectors $\boldsymbol{t}_{43}$ and $\boldsymbol{t}_{45}$, respectively.

The traction force vector $\boldsymbol{t}_a$ can be formulated in terms of $\boldsymbol{v}_a^C$ from the component equations of motion, Eq. (7), and $\boldsymbol{t}_a$ is related back to $\boldsymbol{T}_a$ as indicated in Eq. (4). To use submatrices explicitly, substitute Eqs. (9), (10), and (11) into the component equations of motion, Eq. (7), and then $\boldsymbol{t}_a$ can be algebraically solved as

$$\boldsymbol{t}_a = \boldsymbol{Z}_a \boldsymbol{v}_a^C - \boldsymbol{f}_a \tag{47}$$

where

$$\boldsymbol{Z}_a = \boldsymbol{z}_a^C + \omega^2 \boldsymbol{m}_a^{CN} \boldsymbol{z}_a^{N^{-1}} \boldsymbol{m}_a^{CN^T} \tag{48}$$

$$\boldsymbol{f}_a = \boldsymbol{f}_a^C - j\omega \boldsymbol{m}_a^{CN} \boldsymbol{z}_a^{N^{-1}} \boldsymbol{f}_a^N \tag{49}$$

Here, $\boldsymbol{z}_a^C$ is the impedance matrix of substructure a associated with constraint modes, and $\boldsymbol{z}_a^N$ is the impedance matrix of substructure a associated with component normal modes:

$$\boldsymbol{z}_a^C = (\gamma/\omega)\boldsymbol{k}_a^C + j\left[\omega \boldsymbol{m}_a^C - (1/\omega)\boldsymbol{k}_a^C\right] \tag{50}$$

$$\boldsymbol{z}_a^N = (\gamma/\omega)\boldsymbol{k}_a^N + j\left[\omega \boldsymbol{m}_a^N - (1/\omega)\boldsymbol{k}_a^N\right] \tag{51}$$

The term $\mathrm{Re}[\boldsymbol{v}_a^{C^*} \boldsymbol{\alpha}_{ab}^T \boldsymbol{\alpha}_{ab} \boldsymbol{t}_a]$ in Eq. (44) can be estimated using Eq. (47):

$$\mathrm{Re}\left\{\boldsymbol{v}_a^{C^*} \boldsymbol{\alpha}_{ab}^T \boldsymbol{\alpha}_{ab} \boldsymbol{t}_a\right\} = \boldsymbol{v}_a^{C^*}\, \mathrm{Re}[\boldsymbol{A}_{ab}\boldsymbol{Z}_a]\boldsymbol{v}_a^C - \mathrm{Re}\left[\boldsymbol{v}_a^{C^*} \boldsymbol{A}_{ab} \boldsymbol{f}_a\right] \tag{52}$$

where $\boldsymbol{A}_{ab} = \boldsymbol{\alpha}_{ab}^T \boldsymbol{\alpha}_{ab}$, which is a diagonal matrix with only 0 and 1 in its diagonal elements. In the example shown in Fig. 1, $\boldsymbol{A}_{43}$ will simply be

$$\boldsymbol{A}_{43} = \begin{bmatrix} \boldsymbol{I}_{n_{43}\times n_{43}} & 0_{n_{43}\times n_{45}} \\ 0_{n_{45}\times n_{43}} & 0_{n_{45}\times n_{45}} \end{bmatrix} \tag{53}$$

Now the power flow can be formulated using a basis of either the constraint modes or the CC modes at this level. First, the computational efficiency can be achieved by projecting $\boldsymbol{t}_a$ and $\boldsymbol{v}_a^C$ onto the CC modes. The right-hand side of Eq. (52) is now expressed in terms of CC-mode velocities $\boldsymbol{v}^{CC}$ in place of the constraint-mode velocities at this level $\boldsymbol{v}^C$:

$$\mathrm{Re}\left\{\boldsymbol{v}_a^{C^*} \boldsymbol{\alpha}_{ab}^T \boldsymbol{\alpha}_{ab} \boldsymbol{t}_a\right\} = \boldsymbol{v}_h^{CC^*} \boldsymbol{C}_{ab} \boldsymbol{v}_h^{CC} - \mathrm{Re}\left[\boldsymbol{v}_h^{CC^*} \boldsymbol{f}_{ab}\right] \tag{54}$$

where

$$\boldsymbol{C}_{ab} = \boldsymbol{\Psi}_h^T \boldsymbol{\beta}_a^{\Theta^T}\, \mathrm{Re}[\boldsymbol{A}_{ab}\boldsymbol{Z}_a]\boldsymbol{\beta}_a^{\Theta} \boldsymbol{\Psi}_h \tag{55}$$

$$\boldsymbol{f}_{ab} = \boldsymbol{\Psi}_h^T \boldsymbol{\beta}_a^{\Theta^T} \boldsymbol{A}_{ab} \boldsymbol{f}_a \tag{56}$$

Equation (54) can be evaluated by solving CC-mode velocities $\boldsymbol{v}_h^{CC}$ from Eq. (38), in which $\boldsymbol{v}_h^{CC}$ can be explicitly expressed as

$$\boldsymbol{v}_h^{CC} = \boldsymbol{Y}_h \left(\sum_{a \in I} \boldsymbol{\Psi}_h^T \boldsymbol{\beta}_a^{\Theta^T} \boldsymbol{f}_a \right) \tag{57}$$

where $\boldsymbol{Y}_h$ is the projection of the substructure mobility onto the CC-mode coordinates

$$\boldsymbol{Y}_h = \left(\sum_{a \in I} \boldsymbol{\Psi}_h^T \boldsymbol{\beta}_a^{\Theta^T} \boldsymbol{Z}_a \boldsymbol{\beta}_a^{\Theta} \boldsymbol{\Psi}_h \right)^{-1} \tag{58}$$

Finally, considering deterministic time-harmonic excitation, the power flow can be formulated in terms of $\boldsymbol{v}_h^{CC}$ as

$$\Pi_{ab}(\omega) = \tfrac{1}{2}\,\mathrm{Re}\left[\boldsymbol{v}_h^{CC^*} \boldsymbol{f}_{ab}\right] - \tfrac{1}{2} \boldsymbol{v}_h^{CC^*} \boldsymbol{C}_{ab} \boldsymbol{v}_h^{CC} \tag{59}$$

In addition, for a general broadband random excitation, $\Pi_{ab}(\omega)$ becomes

$$\Pi_{ab}(\omega) = \mathrm{tr}\left[\mathrm{Re}\left(\boldsymbol{S}_{ab}\boldsymbol{Y}_h^*\right) - \boldsymbol{S}_h \boldsymbol{Y}_h^* \boldsymbol{C}_{ab} \boldsymbol{Y}_h\right] \tag{60}$$

where matrices $\boldsymbol{S}_{ab}$ and $\boldsymbol{S}_h$ are given by

$$\boldsymbol{S}_{ab} = -\frac{1}{2\pi} \lim_{T\to 0} \frac{1}{2T} \sum_{a \in I} E_t\left[\boldsymbol{f}_{ab} \boldsymbol{f}_a^* \boldsymbol{\beta}_a^{\Theta} \boldsymbol{\Psi}_h\right] \tag{61}$$

$$\boldsymbol{S}_h = -\frac{1}{2\pi} \lim_{T\to 0} \frac{1}{2T} \sum_{a_1 \in I} \sum_{a_2 \in I} E_t\left[\boldsymbol{\Psi}_h^T \boldsymbol{\beta}_{a_2}^{\Theta^T} \boldsymbol{f}_{a_2} \boldsymbol{f}_{a_1}^* \boldsymbol{\beta}_{a_1}^{\Theta} \boldsymbol{\Psi}_h\right] \tag{62}$$

Next, considering the basis of the constraint modes at this level, $\boldsymbol{v}_h^{\Theta}$ can be solved from Eq. (33) when substructure h is the top-level substructure or from Eq. (34) when substructure h is an intermediate-level substructure:

$$\boldsymbol{v}_h^{\Theta} = \left(\sum_{a \in I} \boldsymbol{\beta}_a^{\Theta^T} \boldsymbol{Z}_a \boldsymbol{\beta}_a^{\Theta} \right)^{-1} \left(\sum_{b \in I} \boldsymbol{\beta}_b^{\Theta^T} \boldsymbol{f}_b \right) \tag{63}$$

By using $\boldsymbol{v}_h^{\Theta}$, the power flow $\Pi_{ab}(\omega)$ can be formulated to be the same form as Eqs. (59) and (60), only without the action of projection to the basis of the CC modes (multiplying by $\boldsymbol{\Psi}_h$).

Numerical Examples

Two simple example structures, a two-span beam and a cantilever plate, are used to illustrate the accuracy and efficiency of the CC-mode-based formulation. Each structure is subjected to rain-on-the-roof random excitation, and Eq. (60) is used to calculate the power flow. The power flow calculated with the CMS model is used as a benchmark for checking the accuracy of the CC-mode-based approximations because a CC-mode-based model will be no more accurate than its parent CMS model.

Two-Span Beam

Consider the simply supported two-span beam presented in Fig. 2. Each span is treated as a substructure, and these substructures are referred to as beam 1 and beam 2. (The modeling of power flow in this system using traditional CMS was examined in detail in an earlier work by the authors.[6]) The dimensions and material properties for each beam are: length 5 m, cross section 0.2 m × 0.1 m, structural damping factor 0.02, Poisson's ratio 0.3, Young's modulus 210 GPa, and density 7200 kg/m^3.

All finite element analyses for this example system were performed using the commercial code ABAQUS. To treat each beam

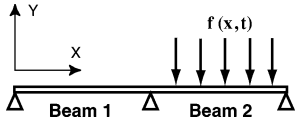

Fig. 2 Two-span beam on simple supports, with each span treated as a substructure.

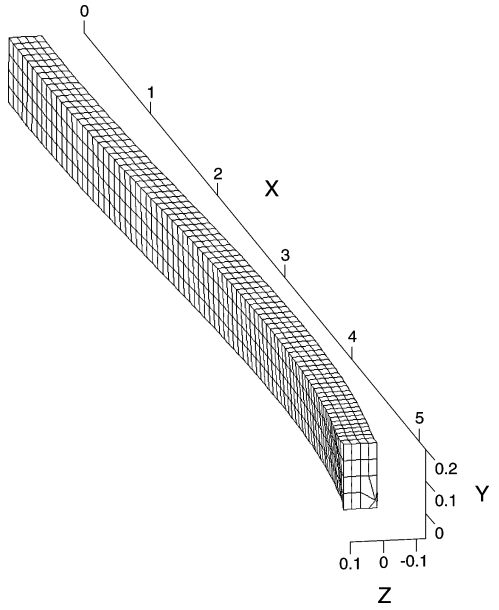

Fig. 3 One of 60 constraint modes for beam 1.

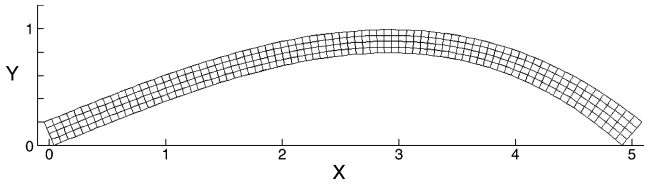

Fig. 4 First CC mode for the beam example (only beam 1 is shown).

as an arbitrary substructure, a general finite element model consisting of three-dimensional solid elements is used. This solid-element FEM has 25 nodes at the interface between beam 1 and beam 2. One horizontal line of nodes in the center of the interface is fixed in order to represent a pinned condition. This leaves 20 unconstrained finite element nodes (60 DOF) in the interface, yielding 60 constraint modes in the CMS model. One of these constraint modes is shown for beam 1 in Fig. 3. Note that Fig. 3 is a rotated view of beam 1, such that the interface is in the foreground.

Now, consider a CMS model in which the component modes are taken to be the first 11 XY-plane flexural modes from the solid-element FEM. For the two beams, this yields 22 component modes. With 60 constraint modes, the Craig–Bampton CMS model has a total of 82 DOF. For the reduced-order model, only the first characteristic constraint mode is included, and so this model has only 23 DOF. The first CC mode is shown in Fig. 4. Note that this CC mode captures XY-plane flexural motion at the interface. In fact, it is identical to the single constraint mode one would obtain using beam elements.[7]

The power flow results are shown in Fig. 5 for the case of beam 2 subjected to rain-on-the-roof random excitation. It can be seen that the results for the ROM with just one CC mode are very close to the results for the CMS model that includes all of the traditional constraint modes. Note that all of the matrices in Eq. (60) have a dimension equal to the number of CC modes included in the model. Thus, for the ROM with one CC mode, all of the quantities become scalar. When performing the frequency sweep calculation for the power flow, the reduction of computational cost is clear, because a scalar equation is now computed as opposed to the matrix equation with a dimension of 60.

Cantilever Plate

The rectangular cantilever plate shown in Fig. 6 is now considered as an example structure. The system properties and substructure partitions are chosen to be the same as those used by Craig

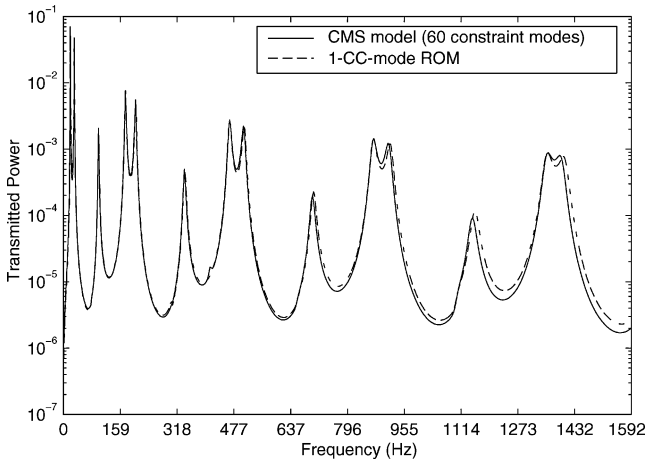

Fig. 5 Power flow between beams 1 and 2.

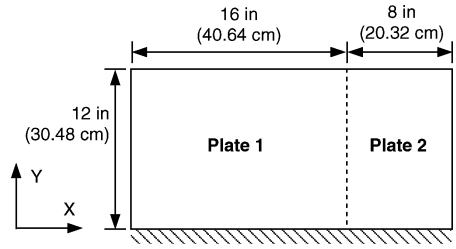

Fig. 6 Cantilever plate partitioned into two substructures.

and Bampton.[4] The material properties and dimensions are 2024-T3 aluminum, Young's modulus 10.5×10^6 psi (72 GPa), Poisson's ratio 0.33, density 0.101 lb/in.^{3} (2800 kg/m^3), structural damping factor 0.02, and thickness 0.125 in. (0.3175 cm). The plate is partitioned into two substructures, referred to as plate 1 and plate 2, with dimensions shown in Fig. 6.

As with the preceding example, ABAQUS was used for all finite element analyses for this structure. A finite element model of the cantilever plate was constructed using shell elements (ABAQUS element S4R, 4 nodes/element, six DOF/node) with a mesh size of $48 \times 24 \times 1$. With this FEM, the first 10 natural frequencies of the cantilever plate are all within 0.7% of the analytical results given by Gorman.[25]

For a CMS model of the plate, the first 10 normal modes are retained for each component structure. In addition, there are 144 constraint modes, yielding a CMS model with 164 DOF. The comparisons of the natural frequencies calculated from the full CMS model and from reduced-order models have been presented previously by the authors.[7] Here, the accuracy of the power flow calculations is considered.

The 164-DOF CMS model provides a high-fidelity model of the frequency response up to about 800 Hz, and so 0–800 Hz was taken as the frequency range of interest. Two reduced-order models were constructed by retaining the lowest four and eight CC modes, which yields ROM sizes of 24 and 28 DOF, respectively. With rain-on-the-roof excitation on plate 1, the power flow from plate 1 to plate 2 was calculated by using the three models. The results are shown in Fig. 7. It can be seen that the results for the four-CC-mode ROM agree well with those of the CMS model up to 500 Hz. Furthermore, the eight-CC-mode ROM has very good agreement with the CMS model throughout the frequency range considered.

Finally, the effect of a particular CC mode on the power flow prediction is considered. It was shown in an earlier work by the authors[7] that the second CC mode captures much of the interface-induced motion seen in the second and third system modes of the cantilever plate. The influence of specific CC modes on the accuracy of the power flow calculations is demonstrated by the results shown in Fig. 8. For Fig. 8a, only the first CC mode is included for the ROM. For Fig. 8b, the second CC mode is also included in the ROM, and

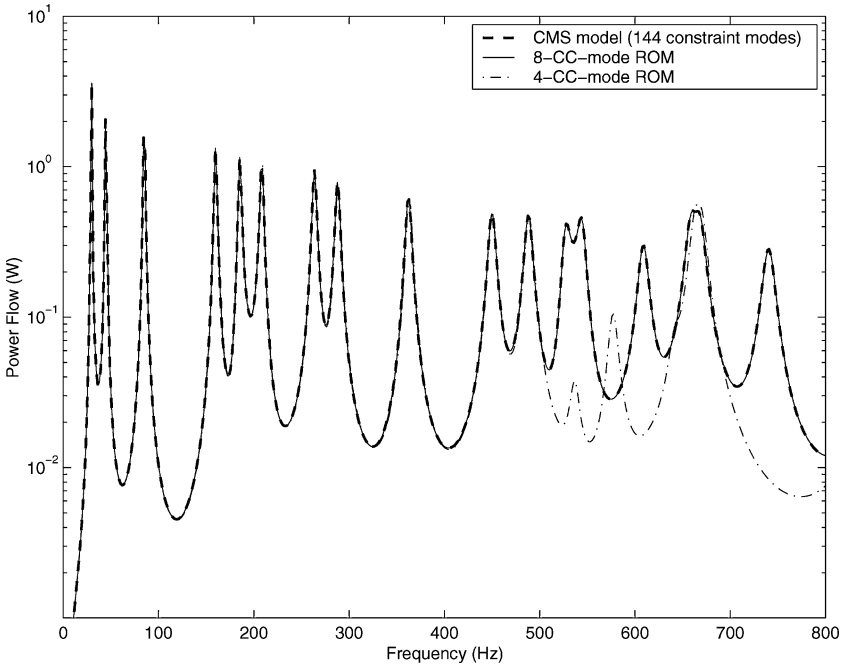

Fig. 7 Power flow between plates 1 and 2.

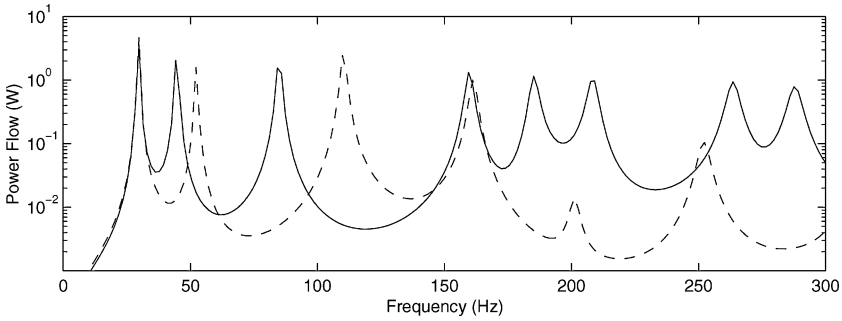

a) CMS model (——) vs 1-CC-mode ROM (– – –)

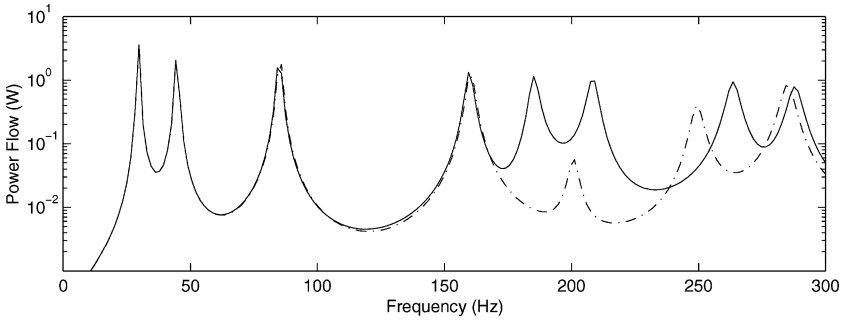

b) CMS model (——) vs 2-CC-mode ROM (· – ·)

Fig. 8 Influence of the first two CC modes on the approximation of power flow in the plate.

this results in the correction of the second and the third peaks of the predicted power flow. This illustrates how the CC modes can provide a basis for predicting power flow with relatively few DOF.

Application: Military Vehicle

The body structure, or hull, for a concept design of a military vehicle is now considered as an example system. Because this is a tracked vehicle, there are several points on each side of the hull where the track system is connected. In this section, the CC-mode-based formulation is used to determine the power flow in the vehicle when it is subjected to excitation at the track system attachment points. The reduced-order model results are compared to those from the full finite element model.

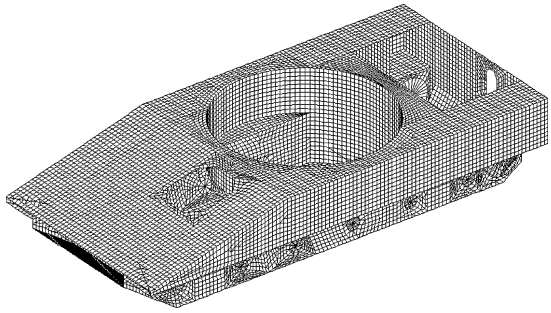

Fig. 9 Finite element mesh for the body structure (hull) of a military vehicle.

For this example structure, the material was taken to be steel with Young's modulus 2.9×10^7 psi (200 GPa), Poisson's ratio 0.3, and density 0.283 lb/in.^{3} (7830 kg/m^3). All finite element analyses for this system were performed using the commercial code MSC/NASTRAN. A finite element model of the body structure was constructed with plate elements of thickness 0.4 in. (1 cm). The mesh is shown in Fig. 9. There are 115,344 DOF in this finite element model. This system features high modal density; there are 385 vibration modes under 500 Hz and 1043 modes under 1000 Hz.

Multilevel Substructuring

For this example, multilevel substructuring is employed. The body structure is first divided into two intermediate-level substructures, the upper and lower hulls, as shown in Fig. 10a. These two substructures are assigned the indices 1 and 2. After removing singular DOF, there are 1816 DOF at the interface between the upper and lower hull. In addition, each component structure still has a large number of interior DOF. Therefore, the intermediate-level substructures are partitioned into a set of bottom-level substructures,

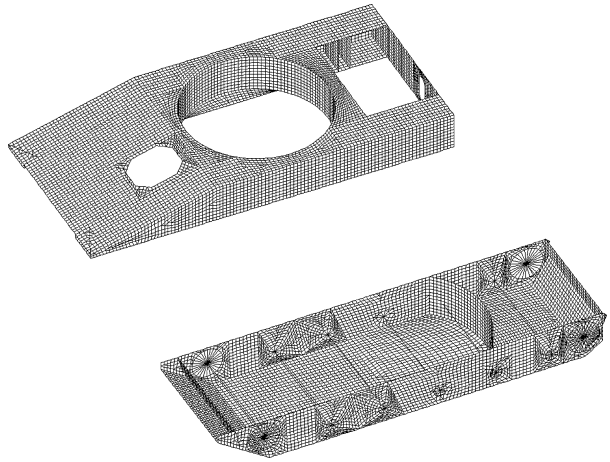

a) Intermediate-level substructures: upper and lower hulls

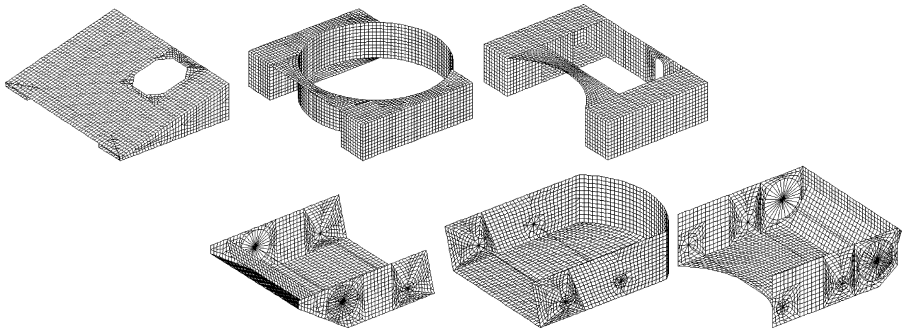

b) Bottom-level substructures

Fig. 10 Multilevel substructuring of the military vehicle.

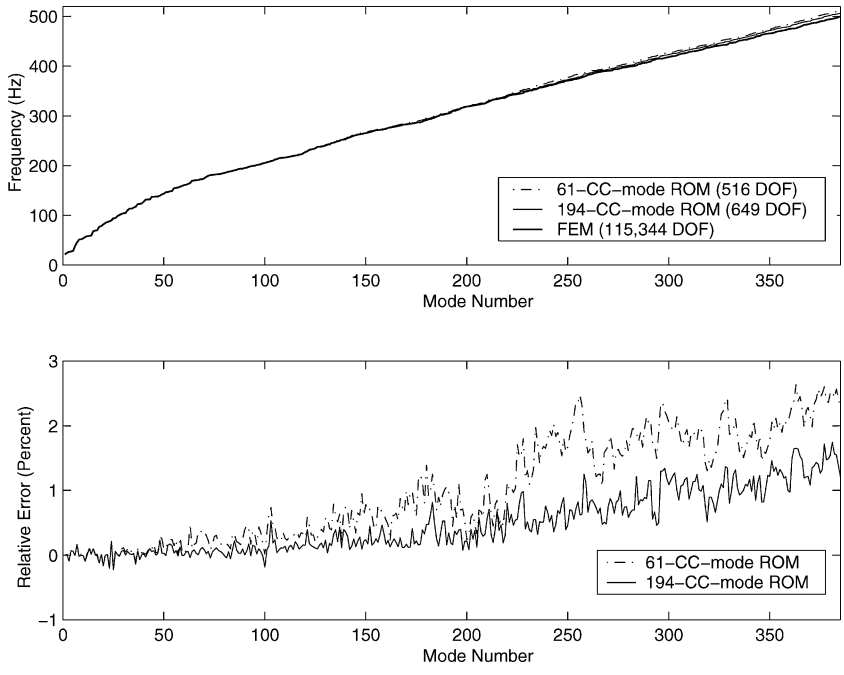

Fig. 11 Accuracy of ROM results, relative to finite element results, for system natural frequencies up to 500 Hz.

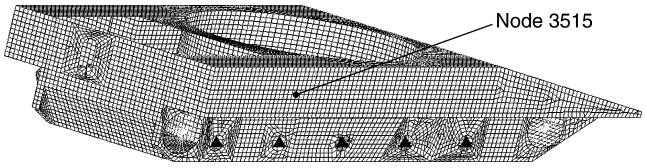

Fig. 12 Location of excitation points (triangles) and response point (node 3515).

as shown in Fig. 10b. The three components of substructure 1 (upper hull) are indexed by 3–5. The three components of substructure 2 (lower hull) are indexed by 6–8.

After this multilevel partitioning, the finite element models of the bottom-level substructures are used to calculate component normal modes and constraint modes. Then, CMS models are assembled for the two intermediate-level substructures, the upper and lower hulls. These models have mass and stiffness matrices of the form of Eqs. (17) and (18).

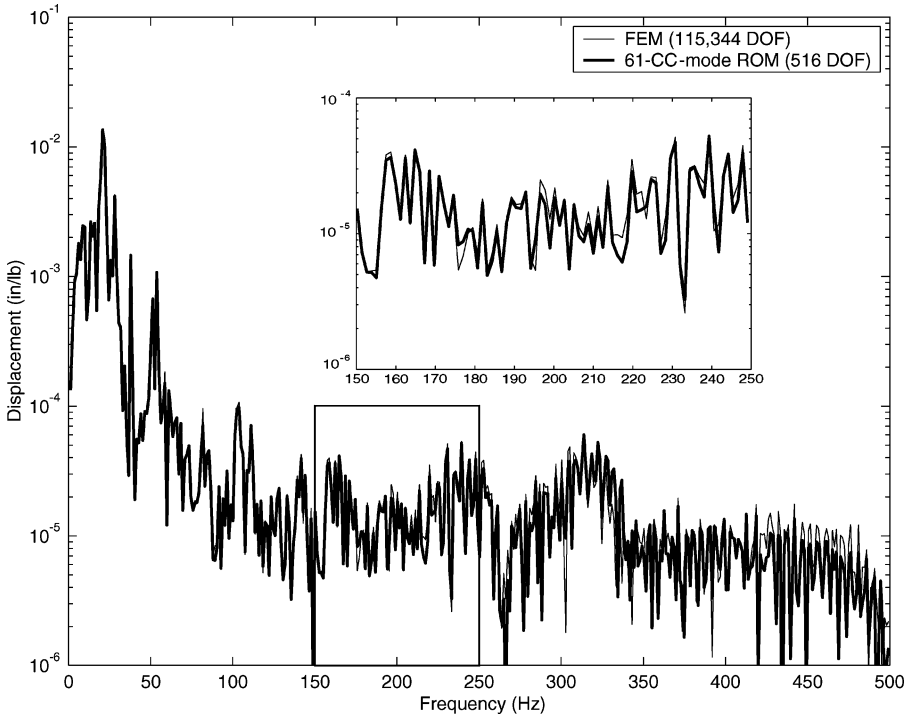

Fig. 13 Vertical displacement at node 3515 per unit load at each excitation point, calculated with the FEM and the 61-CC-mode ROM.

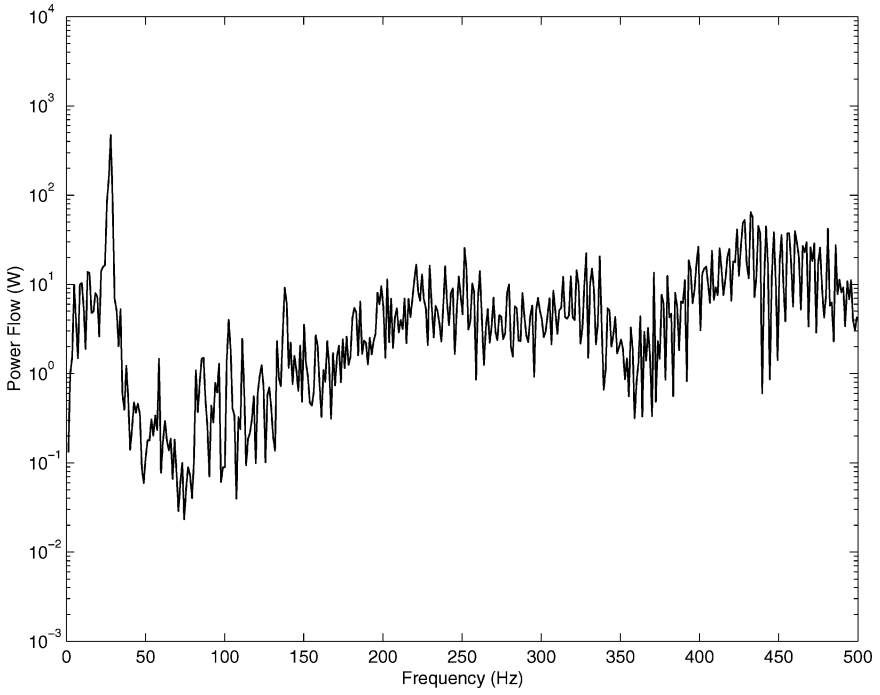

Fig. 14 Power flow from the lower to upper hull, calculated with the 61-CC-mode ROM.

Next, these two intermediate-level models are synthesized to obtain a CMS model [Eq. (16)] of the top-level substructure, which is the entire vehicle body structure. Because there are 1816 DOF in the interface between the upper and lower hull, there are 1816 constraint modes for this CMS model. In addition, 449 component modes and six rigid-body modes are included in the CMS model, in order to capture vibration in the frequency range 0–500 Hz. Thus, the CMS model has 2271 DOF, about 80% of which correspond to the constraint modes.

Free Response

With the use of the CMS model of the top-level substructure, the CC modes are calculated. Two reduced-order models are generated by selecting the lowest 61 and 194 CC modes, yielding ROM sizes of 516 DOF and 649 DOF, respectively. In Fig. 11, the system natural frequencies up to 500 Hz calculated from these two ROMs are compared with those calculated from the full finite element model. Both the actual values and the errors of the ROM natural frequencies relative to the FEM results are shown. As expected, including more CC modes provides more accurate results. Still, the error of the ROM with only 61 CC modes remains below 3% for this frequency range.

Forced Response and Power Flow

For a forced response case, a unit harmonic load was applied in the vertical direction at each point where the suspension system is connected to the body. For reference, the excitation points on one side of the vehicle are shown in Fig. 12. In addition, a node in the upper hull was chosen as a response point for comparing FEM and ROM vibration predictions. This response point, node 3515, is also shown in Fig. 12. The damping for the system was taken to be modal damping, with the damping factor varying linearly from 0.063% at 10 Hz to 3.1% at 500 Hz.

The frequency response results for the vertical displacement of node 3515 calculated by the full FEM and the 61-CC-mode ROM are shown in Fig. 13. It is seen that this 516-DOF ROM is quite accurate relative to the 115,344-DOF FEM for predicting the forced response up to 500 Hz.

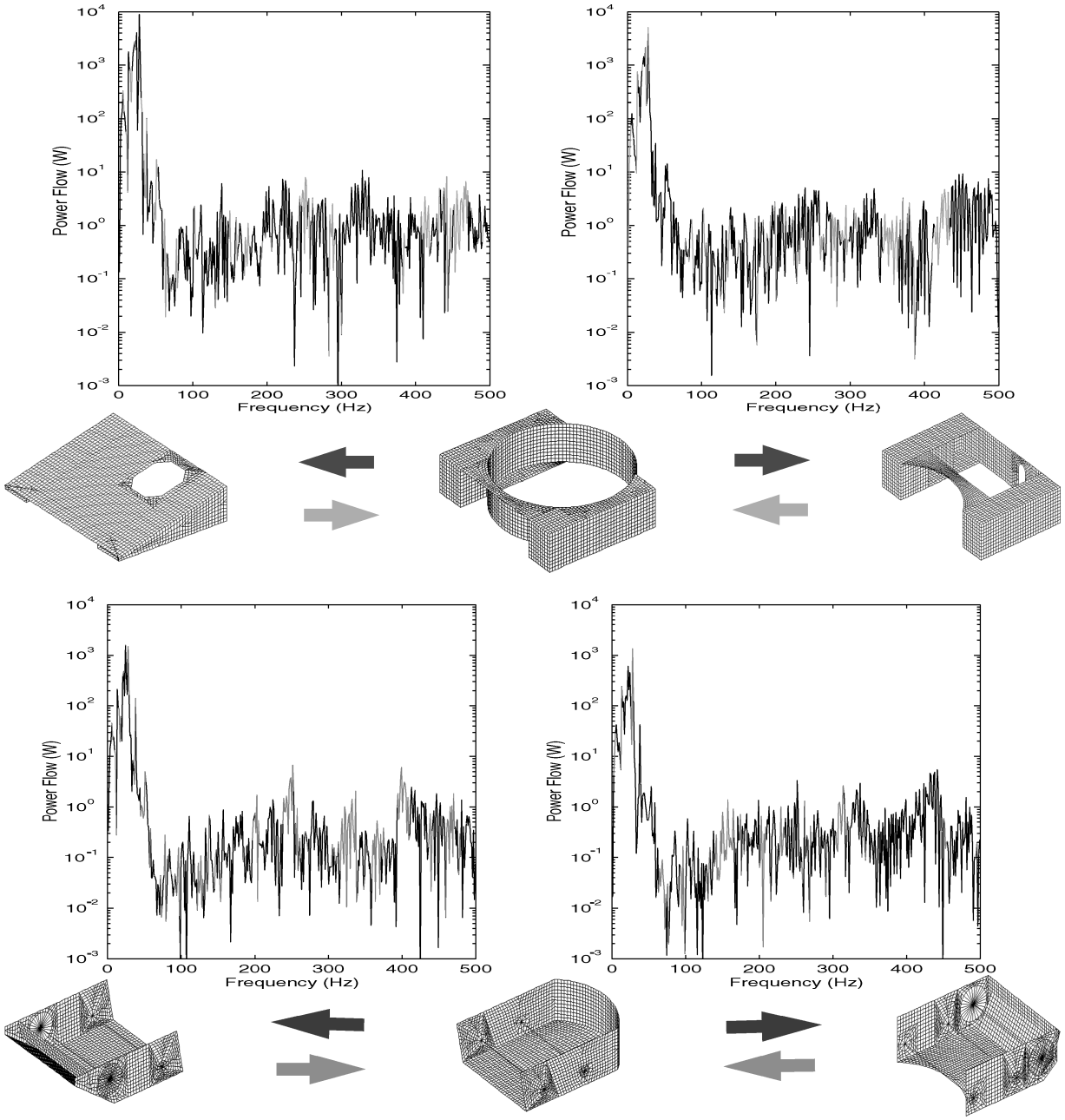

Fig. 15 Power flow inside the upper and lower hulls, calculated with the 61-CC-mode ROM.

Furthermore, this ROM allows the calculation of power flow from the lower to the upper hull. Equation (59) is used for the calculation, and the matrices for this case have a dimension of 61. The predicted power flow is shown in Fig. 14.

Finally, power flow information can be extracted from the CMS models of the two intermediate-level substructures, the upper and lower hulls. Equation (34) governs the motion of these two substructures. The procedure is summarized briefly as follows. First, CC modes $\boldsymbol{\Psi}_1$ and $\boldsymbol{\Psi}_2$ were computed on regions Θ_1 and Θ_2, where 48 and 35 CC modes were kept, respectively. The velocities $\boldsymbol{v}_1^{\Gamma}$ and $\boldsymbol{v}_2^{\Gamma}$ were mapped from the CC-mode velocities of the top-level substructure in order to calculate the modified force $\tilde{\boldsymbol{f}}_1^{\Omega}$ and $\tilde{\boldsymbol{f}}_2^{\Omega}$. Next, the CC modes $\boldsymbol{\Psi}_1$ and $\boldsymbol{\Psi}_2$ were used to transform Eq. (34) into Eq. (38) such that reduced-order models for calculating the power flow within substructures 1 and 2 were obtained. The power flow inside the upper and lower hulls is shown in Fig. 15. Each frequency response plot represents the power flow between a pair of connected substructures, and the direction of the power flow is indicated by the arrow corresponding to the color of the plotted line. Together, Figs. 14 and 15 provide a map of the power flow in the vehicle structure.

Conclusions

This paper examined the use of component mode synthesis (CMS) to formulate modal approximations of power flow in complex structures, based on finite element models of the components. It was noted that the Craig–Bampton method of CMS provides a good basis for evaluating power flow between component structures because the constraint modes evidence the motion at the interface, which is used for computing the power flow. However, the number of DOF caused by the constraint modes can make the CMS model inefficient for calculating the power flow. Therefore, a method was employed for computing characteristic constraint (CC) modes. It was seen that the CC modes identified the fundamental vibration transmission mechanisms for the system. Thus, a subset of these characteristic constraint modes can be selected to yield a reduced-order model for computing the power flow. Power flow analyses were performed on example systems of a two-span beam and a cantilever plate. It was seen that the results using reduced-order models agreed well with the results using the parent CMS models. In addition, the body structure of a military vehicle was considered as an example. A multilevel substructuring technique was used to generate a highly reduced-order model, and the power flow in the vehicle structure was tracked using CC-mode-based models at each level of substructuring. This type of power flow analysis can be used to predict substructure vibration levels, to identify critical paths of vibration energy transmission, and to provide information for possible design changes.

Acknowledgments

The authors gratefully acknowledge the support of the Automotive Research Center, a U.S. Army TACOM center of excellence for modeling and simulation of ground vehicles at the University of Michigan. In addition, the authors thank Zheng-Dong Ma for generating the finite element model of the military vehicle and providing benchmark results from MSC/NASTRAN.

References

[1]Lyon, R. H., *Statistical Energy Analysis of Vibrating Systems*, MIT Press, Cambridge, MA, 1975.

[2]Lyon, R. H., and DeJong, R. G., *Theory and Application of Statistical Energy Analysis*, Butterworth–Heinemann, Boston, 1995.

[3]Hurty, W. C., "Dynamic Analysis of Structural Systems Using Component Modes," *AIAA Journal*, Vol. 3, No. 4, 1965, pp. 678–685.

[4]Craig, R. R., Jr., and Bampton, M. C. C., "Coupling of Substructures for Dynamic Analyses," *AIAA Journal*, Vol. 6, No. 7, 1968, pp. 1313–1319.

[5]Craig, R. R., Jr., *Structural Dynamics: An Introduction to Computer Methods*, Wiley, New York, 1981, Chap. 19.

[6]Tan, Y. C., Castanier, M. P., and Pierre, C., "Approximations of Power Flow Between Two Coupled Beams Using Statistical Energy Methods," *Journal of Vibration and Acoustics*, Vol. 123, No. 4, 2001, pp. 510–523.

[7]Castanier, M. P., and Tan, Y. C., and Pierre, C., "Characteristic Constraint Modes for Component Mode Synthesis," *AIAA Journal*, Vol. 39, No. 6, 2001, pp. 1182–1187.

[8]Craig, R. R., Jr., and Chang, C.-J., "Substructure Coupling for Dynamic Analysis and Testing," NASA CR-2781, Feb. 1977.

[9]Bourquin, F., and d'Hennezel, F., "Intrinsic Component Mode Synthesis and Plate Vibrations," *Computers and Structures*, Vol. 44, No. 1–2, 1992, pp. 315–324.

[10]Bourquin, F., and d'Hennezel, F., "Numerical Study of an Intrinsic Component Mode Synthesis Method," *Computer Methods in Applied Mechanics and Engineering*, Vol. 97, No. 1, 1992, pp. 49–76.

[11]Balmès, E., "Optimal Ritz Vectors for Component Mode Synthesis Using the Singular Value Decomposition," *AIAA Journal*, Vol. 34, No. 6, 1996, pp. 1256–1260.

[12]Brahmi, K., and Bouhaddi, N., "Improved Component Mode Synthesis Based on Double Condensation Method," *Proceedings of the 15th International Modal Analysis Conference*, Vol. 2, Society for Experimental Mechanics, Bethel, CT, 1997, pp. 1469–1475.

[13]Jacobsen, K. P., "Fully Integrated Superelements: A Database Approach to Finite Element Analysis," *Computers and Structures*, Vol. 16, No. 1–4, 1983, pp. 307–315.

[14]Elwi, A. E., and Murray, D. W., "Skyline Algorithms for Multilevel Substructure Analysis," *International Journal for Numerical Methods in Engineering*, Vol. 21, No. 3, 1985, pp. 465–479.

[15]Prakash, B. G., and Prabhu, M. S. S., "Reduction Techniques in Dynamic Substructures for Large Problems," *Computers and Structures*, Vol. 22, No. 4, 1986, pp. 539–552.

[16]Bennighof, J. K., and Kaplan, M. F., "Frequency Window Implementation of Adaptive Multi-Level Substructuring," *Journal of Vibration and Acoustics*, Vol. 120, No. 2, 1998, pp. 409–418.

[17]Bennighof, J. K., and Kaplan, M. F., "Frequency Sweep Analysis Using Multi-Level Substructuring, Global Modes and Iteration," *Proceedings of the 39th AIAA/ASME/ASCE/AHS/ASC Structures, Structural Dynamics, and Materials Conference and Exhibit*, Vol. 4, AIAA, Reston, VA, 1998, pp. 2567–2575.

[18]Bennighof, J. K., Kaplan, M. F., and Muller, M. B., "Reducing NVH Analysis Burden Using Automated Multi-Level Substructuring," *Proceedings of the 17th International Modal Analysis Conference*, Vol. 1, Society for Experimental Mechanics, Bethel, CT, 1999, pp. 372–377.

[19]Bennighof, J. K., Kaplan, M. F., Muller, M. B., and Kim, M., "Meeting the NVH Computational Challenge: Automated Multi-Level Substructuring," *Proceedings of the 18th International Modal Analysis Conference*, Vol. 1, Society for Experimental Mechanics, Bethel, CT, 2000, pp. 909–915.

[20]Mourelatos, Z. P., "An Efficient Crankshaft Dynamic Analysis Using Substructuring with Ritz Vectors," *Journal of Sound and Vibration*, Vol. 238, No. 3, 2000, pp. 495–527.

[21]Nefske, D. J., and Sung, S. H., "Power Flow Finite Element Analysis of Dynamic Systems: Basic Theory and Application to Beams," *Journal of Vibration, Acoustics, Stress and Reliability in Design*, Vol. 111, No. 1, 1989, pp. 94–100.

[22]Wohlever, J. C., and Bernhard, R. J., "Mechanical Energy Flow Models of Rods and Beams," *Journal of Sound and Vibration*, Vol. 153, No. 1, 1992, pp. 1–19.

[23]Bouthier, O. M., and Bernhard, R. J., "Models of Space-Averaged Energetics of Plates," *AIAA Journal*, Vol. 30, No. 3, 1992, pp. 616–623.

[24]Mace, B. R., and Shorter, P. J., "Energy Flow Models from Finite Element Analysis," *Journal of Sound and Vibration*, Vol. 233, No. 3, 2000, pp. 369–389.

[25]Gorman, D. J., *Free Vibration Analysis of Rectangular Plates*, Elsevier, New York, 1982, Chap. 4.

A. Berman
Associate Editor